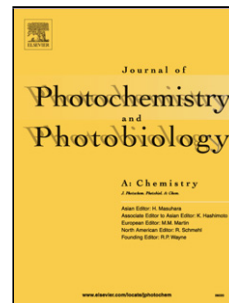


Accepted Manuscript

Title: A nitrogen-doped porous carbon derived from copper phthalocyanines on/in ZIF-8 as an efficient photocatalyst for the degradation of dyes and the C-H activation of formamides

Authors: Siyavash Kazemi Movahed, Zeinab Piraman, Minoos Dabiri



PII: S1010-6030(17)30833-X
DOI: <https://doi.org/10.1016/j.jphotochem.2017.10.026>
Reference: JPC 10951

To appear in: *Journal of Photochemistry and Photobiology A: Chemistry*

Received date: 14-6-2017
Revised date: 13-10-2017
Accepted date: 14-10-2017

Please cite this article as: Siyavash Kazemi Movahed, Zeinab Piraman, Minoos Dabiri, A nitrogen-doped porous carbon derived from copper phthalocyanines on/in ZIF-8 as an efficient photocatalyst for the degradation of dyes and the C-H activation of formamides, *Journal of Photochemistry and Photobiology A: Chemistry* <https://doi.org/10.1016/j.jphotochem.2017.10.026>

This is a PDF file of an unedited manuscript that has been accepted for publication. As a service to our customers we are providing this early version of the manuscript. The manuscript will undergo copyediting, typesetting, and review of the resulting proof before it is published in its final form. Please note that during the production process errors may be discovered which could affect the content, and all legal disclaimers that apply to the journal pertain.

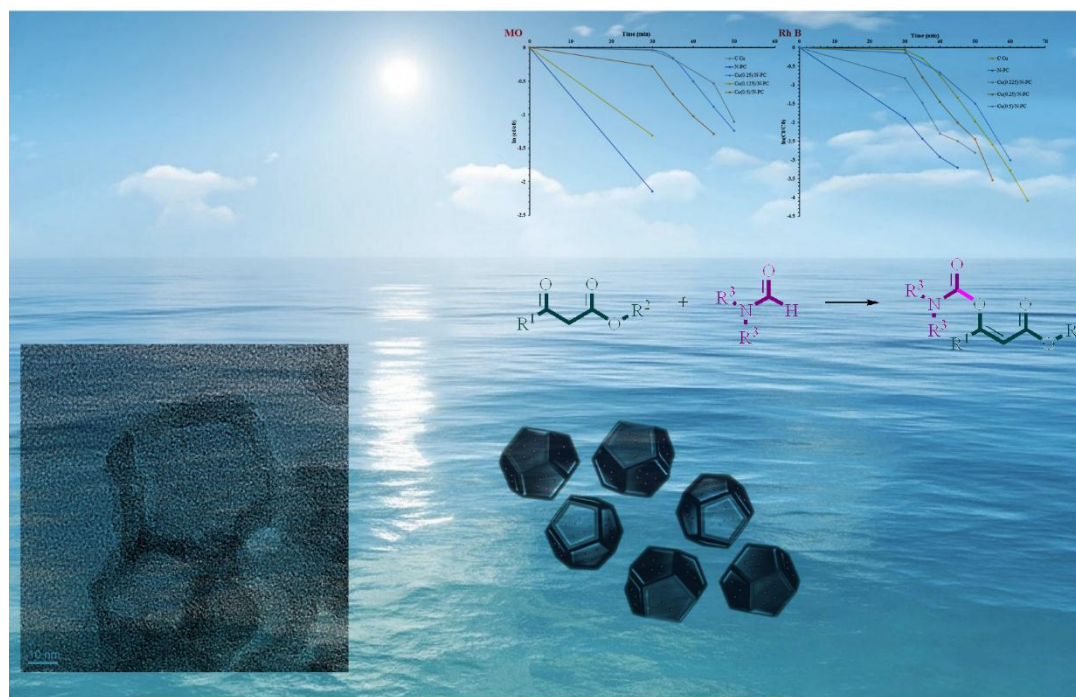
A nitrogen-doped porous carbon derived from copper phthalocyanines on/in ZIF-8 as an efficient photocatalyst for the degradation of dyes and the C-H activation of formamides

Siyavash Kazemi Movahed, Zeinab Piraman, and Minoos Dabiri*

Shahid Beheshti University, Tehran, Islamic Republic of Iran. Fax: +98 21 22431661; Tel: +98

21 29903255; E-mail: m-dabiri@sbu.ac.ir

Graphical abstract



Highlights

1. A novel doped carbon from the carbonization of the CuPc on/in ZIF-8 hybrid.
2. The weight ratio of CuPc / ZIF-8 in the catalyst was studied in the behavior catalyst

3. The weight ratios 1:2 and 1:8 of CuPc / ZIF-8 showed the high dye absorption activity
4. The weight ratio 1:4 demonstrated the high photocatalytic activity
5. The C-H activation of formamides within 30 min under the solar-simulated light, in the presence 0.02 mol% of Cu.

Abstract

A novel nitrogen doped carbon photocatalyst was successfully prepared from the carbonization of copper phthalocyanine (CuPc) on/in zeolitic imidazolate framework-8 (ZIF-8) hybrid. Carbonized catalysts derived from either ZIF-8 or CuPc exhibit poor activity towards the degradation of dyes (such as methyl orange (MO) and Rhodamine B (Rh B)), whereas carbonized CuPc complex supported on ZIF-8 exhibits extremely high performance. The weight ratios 1:2 and 1:8 of CuPc/ZIF-8 showed the high dye absorption activity, while the weight ratio 1:4 demonstrated the high photocatalytic activity in the presence of H₂O₂ as an oxidant. For the first time, the photocatalyst (Cu/N-PC) was used in C-H activation of formamides in the presence of *tert*-butyl hydroperoxide (TBHP) as an oxidant. The reaction proceeded within 30 min, in the presence 0.02 mol% of Cu.

Keywords: Heterogeneous catalysis; Photocatalysis; Degradation; C-H bond activation; Nanostructure.

1. Introduction

Porous carbon, a class of non-oxide porous materials, provide unique characteristics such as chemical inertness, easy availability, excellent mechanical and thermal stability, high specific surface area, low density, large pore volumes, and surface hydrophobicity [1-3].

Porous carbon exhibit broad application including batteries [4], catalyst supports [5], chromatography columns [6], gas separation [7], fuel cells [8], and water purification [9]. It has been proved that heteroatom doping (e.g., boron, nitrogen, phosphorus, sulfur, etc.) inside the frame of porous carbons is robust access to tuning electronic properties or/and electrical conductivity, as well as electron-donor tendency of the porous carbons [10-13].

Metal–organic frameworks (MOFs) are a class of porous crystalline materials that consist of coordination bonds between transition-metal cations (nodes) and multitopic organic ligands (linkers). In the last decade, MOFs have attracted worldwide attention due to their topology, high surface area, high porosity, and low density. These materials have potential applications in catalysis, sensing, clean energy, chemical separations, gas storage, drug delivery, biomedical imaging, electron, ion, proton conduction and so on [14-16]. Recently, MOFs have been shown as new templates and reactive precursors to make porous carbons by direct calcination in an inert atmosphere [17]. Zeolitic imidazolate frameworks (ZIFs), a subclass of MOFs, are constructed from tetrahedral units, in which each metal atom like Zn^{2+} or Co^{2+} connects four imidazolate (im^-) ligands [18]. Different from their MOF analogs with carboxyl-ligands, ZIFs not only exhibit exceptional thermal and chemical stability but also contain a rich nitrogen source in the imidazolate ligands. All these properties make ZIFs an excellent candidate for the construction of *N*-doped porous carbons with superior performances [19,20].

Metal Phthalocyanines (MPcs) as important industrial pigments have been attracted considerably remarkable due to excellent catalytic capability, low cost, negligible toxicity, high chemical, photo and thermal stability, facile preparation on a large scale, semiconducting properties, and most importantly intensive absorption in the red/near-

infrared region [21,22]. MPc as an organometallic semiconductor is the widely used photosensitizer for the generation of singlet oxygen ($^1\text{O}_2$) because they can collect up to 50% of the energy available in the solar spectrum [23]. The catalytic performance of MPc catalyst is limited by the aggregation tendency from large intrinsic π -conjugation, which would self-association or negatively produce inactive dimers. Additionally, the catalyst may also be deactivated *via* self-photodecomposition of MPc during the catalytic oxidation [24]. To solve these issues, supports like the carbon nanotube, chitosan, graphene and fibrous materials, including cellulose and silk have been used to immobilize MPc [25].

Herein, we report the novel protocol for the photocatalytic degradation of dyes and the C-H activation of formamides by Cu/N-PC composite under the solar-simulated light. The synthetic procedure of Cu/N-PC composite is illustrated in Scheme 1. Initially, the CuPc@ZIF-8 composite was synthesized through a solvent-impregnation together with milling. The CuPc was dispersed over the surface or/and filled the micropores of ZIF-8. Finally, the CuPc@ZIF-8 was vacuum dried and carbonized at 900°C under the inert atmosphere. The weight ratio of CuPc/ZIF-8 may be one of the key parameters affecting the impregnated/covered of copper species in/on the ZIF-8 as well as the catalytic activity. In this study, different weights of CuPc were added into a fixed amount of ZIF-8 to investigate CuPc/ZIF-8 weight ratio in the formation of CuPc@ZIF-8 and subsequently, final carbonized catalyst.

2. Experimental

2.1. Synthesis of copper phthalocyanine

The mixtures of phthalonitrile (10 mmol), ammonium heptamolybdate (0.01 mmol), anhydrous copper(I) chloride (2.6 mmol) and nitrobenzene (15 mL) in a Schlenk flask was degassed several times and refluxed under the nitrogen atmosphere (190 °C) for 4h. After cooling to room temperature, the resulting mixture was dispersed in 80 mL toluene and washed with 100 mL deionized water, 300 mL sodium hydroxide 5%, 300 mL hydrochloric acid 10%, 400 mL deionized water and 100 mL acetone, respectively. The greenish blue powder was dissolved in sulfuric acid 98% and precipitated in H₂O. The resulting precipitate was dried at 70 °C [26].

2.2. Synthesis of ZIF-8

2-Methylimidazole (2-MeIm) (56 mmol, 100 mL of methanol solution) was dropping added to zinc nitrate hexahydrate (7 mmol, 100 mL of methanol solution) and stirred for 5 minutes, then stand for 1h at room temperature. The resulting milky solution was centrifuged and washed with methanol for 3 times and dried under vacuum [27].

2.3. Synthesis of Cu_x/N-PC

To prepare the Cu_x/N-PC in different mass ratio, ZIF-8 (100 mg) was added to X (= 50, 25, and 12.5) mg of CuPc (in methanol (10 mL)) and homogenized by sonication for 1 h, and then milled in a mortar for 1h. After drying under vacuum, the resulting composite (CuPc_x@ZIF-8) was transferred into a quartz tube and carbonized at 900 °C for 3 h with a heating rate of 5 °C min⁻¹ and kept at 900 °C for 2h under Ar flow (yield = ~20%). The carbonized composite was sonicated in H₂SO₄ (1M) for 2h and continuously stirred at room temperature for 20 h to remove unstable species (yield = ~ 90%). The resulting mixture was washed with deionized water and dried at 70 °C. Finally, the sample was carbonized at the

same heating rate and kept at 900 °C for 0.5h under Ar flow (yield = ~ 40% and overall yield = ~ 7%).

2.4. Dye photodegradation reaction

The solution of dye (MO (64 mg/L, 18.5 mL) or Rh B (16 mg/L, 18.5 mL)) and composite (0.002 g) were added in a beaker under a constant stirring condition at 500 rpm.min⁻¹ at room temperature under dark conditions for 0.5 h to obtain a good adsorption–desorption equilibrium between the dye molecules and the catalyst surface. After adding H₂O₂ (1.5 mL) and exposing to a Xe lamp, 4 mL of solution separated and the concentration of dye was determined and recorded with a UV-Vis spectrophotometer (at $\lambda_{MO} = 465$ nm or $\lambda_{Rh\ B} = 554$ nm), every 5 minutes.

2.5. Dye absorption test in the dark

This experiment was performed to indicate that the dye was adsorbed in the dark even in the presence of the catalyst, also the light was essential for efficient degradation: the solution of dye (MO (64 mg/L, 18.5 mL) or Rh B (16 mg/L, 18.5 mL)) was added in a beaker contain composite (0.002 g) and magnetically stirred at 500 rpm.min⁻¹ at room temperature in the dark, every 5 minutes 4 mL of solution separated and the concentration of dye was determined and recorded with a UV-Vis spectrophotometer(at $\lambda_{MO} = 465$ nm or $\lambda_{Rh\ B} = 554$ nm).

2.6. General Procedure for the synthesized of enol carbamates

β -ketoester derivative (2 mmol), formamide (54 mmol), TBHP (12 mmol) and composite (0.02 mol% of Cu) were mixed in a round-bottom flask (10 mL). The resulting mixture stirred at 70 °C, exposed a Xe lamp, and the reaction monitored by thin layer chromatography (TLC). After the compilation of reaction, the reaction mixture was cooled

to room temperature; the organic phase was dried over anhydrous Na_2SO_4 and filtered. The crude reaction was concentrated under vacuum. The residue was purified by silica-gel thin layer chromatography using *n*-hexane/ethyl acetate (10:1) as eluent to afford the pure product.

3. Results and discussion

3.1. Characterization

Raman spectroscopy is a powerful technique to investigate the local structure of carbonaceous materials [28]. The Raman spectra of *N*-PC, $\text{Cu}_{0.125}/\text{N-PC}$, $\text{Cu}_{0.25}/\text{N-PC}$, and $\text{Cu}_{0.5}/\text{N-PC}$ composites are shown in Fig. 1. All composites exhibited G and D bands in the Raman spectra. The G band at around 1570 cm^{-1} correspond to sp^2 -carbon in graphite structures and the graphitization. The D band at around 1340 cm^{-1} correspond to sp^3 -carbon in disordered carbon structures or doped heteroatoms [29]. The I_D/I_G ratio increases from 1.13 to 1.19, 1.21, and 1.23 by increasing the weight ratio of $\text{CuPc}_X/\text{ZIF-8}$ from $X=0$, 0.125, 0.25 to 0.5, which suggested a high concentration of defects, which possibly caused by the heteroatom copper [27]. Additionally, the D band enhancement indicates the interaction between the metal nanoparticles and graphite layer that occurs due to the preferential growth of nanoparticles at graphite layer vacancies [30].

XRD measurement was done to study the crystal structure of the ZIF-8, (Fig. 2). The sample exhibited pure crystal with the cubic $I43m$ group, which matched with the well-known ZIF-8 crystal structure. After the carbonization of ZIF-8 at $900\text{ }^\circ\text{C}$, the broad diffraction peak centered at $2\theta = 25^\circ$ appeared and assigned to (0 0 2) lattice plane of the

graphitic carbon. Additionally, the absence of the diffraction peaks of Zn and ZnO impurities indicates that Zn species vaporized away along with the Ar flow during the thermal treatment process [31]. The XRD pattern of the carbonized CuPc (C Cu) includes two sets of peaks. The first one is constituted by three peaks, situated at $2\theta = 43.22^\circ$, 50.37° and 73.99° can be assigned to the (1 1 1), (2 0 0) and (2 2 0) lattice planes of Cu (0). The second set of peaks located at $2\theta = 36.16^\circ$ and 42.14° , could be assigned to the (1 1 1) and (2 0 0) lattice planes of Cu₂O. The appearance of the lattice planes of Cu (0) must arise from reduction to Cu (0) due to decomposition/deligation during high-temperature treatment which was consistent with previous reports [32,33]. An apparent broad peak at $2\theta = 25^\circ$ has been recorded, which assigned to the (0 0 2) facet of the graphitic carbon. The XRD patterns of Cu_{0.125}/*N*-PC, Cu_{0.25}/*N*-PC, and Cu_{0.5}/*N*-PC composites showed a broad peak for graphitic carbon at $2\theta = 25^\circ$ and a set peaks for Cu₂O at $2\theta = 36.22^\circ$, 42.18° , 61.32° , and 73.26° , which could be assigned to the (1 1 1), (2 0 0), (2 2 0) and (3 1 1) lattice planes of Cu₂O. The absence of the diffraction peaks of metallic Cu showed that it was readily oxidized in air to form Cu₂O. Notably, the set peaks for Cu₂O in the XRD pattern of Cu_{0.25}/*N*-PC was strong and sharp, while those in Cu_{0.125}/*N*-PC and Cu_{0.5}/*N*-PC appeared to be weak, which suggested Cu₂O in Cu_{0.25}/*N*-PC has a high crystalline degree. Additionally, the peaks at $2\theta = 44^\circ$ and 64° correspond to stainless steel sample holder of powder diffractometer.

The isotherm of all composites exhibits a type-IV curve according to the IUPAC classification, which suggests the existence of mesopores (Fig. 3). After Cu doping in *N*-PC, the type of hysteresis loop was changed from type-I to type-III that indicated altering the shape of the pores and increasing the non-uniformity size and shape the pores [34]. BET

surface area decreased dramatically from 1613.61 in *N*-PC to 868.89, 585.75 and 256.08 m^2g^{-1} in $\text{Cu}_{0.125}/\text{N-PC}$, $\text{Cu}_{0.25}/\text{N-PC}$, and $\text{Cu}_{0.5}/\text{N-PC}$ composites, respectively. Additionally, the pore volume dropped from 1.23 to 1.05, 0.58 and 0.33 m^3g^{-1} in $\text{Cu}_{0.125}/\text{N-PC}$, $\text{Cu}_{0.25}/\text{N-PC}$, and $\text{Cu}_{0.5}/\text{N-PC}$ composites, respectively (Table 1). These results indicate that the most pores of *N*-PC were impregnated with the Cu, or the Cu was well distributed on/in the *N*-PC composite.

The morphologies of all composites were characterized by the field emission scanning electron microscopy (FESEM). ZIF-8 owns a typical rhombic structure with an average size of 70 nm (Fig. 4a). After carbonization, the obtained *N*-PC retained the parent ZIF-8 morphology, but the some shrinking and deforming were observed as well (Fig. 4b). The impregnation/covering of Cu in/on the *N*-PC did not affect the morphology of $\text{Cu}_{0.125}/\text{N-PC}$ and $\text{Cu}_{0.25}/\text{N-PC}$ composites (Figs. 4c-d). The agglomeration in the morphology of carbonized catalyst was observed by the increasing of amount CuPc into the ZIF-8 ($\text{Cu}_{0.5}/\text{N-PC}$) (Fig. 4e).

The TEM images of *N*-PC and $\text{Cu}_x/\text{N-PC}$ composites showed in Fig. 5 and Figs. S5 and S7. The TEM image of *N*-PC revealed partially destroyed ZIF-8 morphologies, with distorted graphite structures and only a few oriented multilayer graphene domains were observed (Figs 5a-b), which was consistent with the previous reports [35]. $\text{Cu}_x/\text{N-PC}$ composites exhibit a hollow bowl-like morphology (Fig. 5 c-j).

The photoelectrochemical properties and the electronic band structure of all composites were further investigated through diffuse reflectance spectroscopy (DRS) (Fig.

6a). The distinct absorption ability was observed in the visible light region. All $\text{Cu}_x/\text{N-PC}$ composites showed the enhanced visible light absorption in contrast to the *N-PC* and *C Cu*. The $\text{Cu}_{0.5}/\text{N-PC}$ composite exhibit the strongest visible light absorption among all samples. The band gap energy (E_g) was estimated from the intercept of the tangents to the plots of $(ah\nu)^2$ vs. photon energy (Fig. 6b), and the calculated E_g value of *C Cu*, *N-PC*, $\text{Cu}_{0.125}/\text{N-PC}$, $\text{Cu}_{0.25}/\text{N-PC}$, and $\text{Cu}_{0.5}/\text{N-PC}$ composites are around 2.91, 2.83, 2.79, 2.58, and 2.49, respectively.

3.1. The photocatalytic activity of $\text{Cu}_x/\text{N-PC}$ composites on the degradation of MO and Rh B

The photocatalytic activity of the composites on the degradation of MO dye under the solar-simulated light was investigated (Fig. 7). First, the reaction mixture was stirred in the dark for 30 min to complete the adsorption/desorption equilibration of the organic dye by the composites. The *C Cu*, *N-PC*, $\text{Cu}_{0.125}/\text{N-PC}$, $\text{Cu}_{0.25}/\text{N-PC}$, and $\text{Cu}_{0.5}/\text{N-PC}$ composites absorbed around 3.65%, 88.25%, 72.98%, 3.14%, and 65.72% of MO, respectively, in 30 min dark. The *N-PC*, $\text{Cu}_{0.125}/\text{N-PC}$, and $\text{Cu}_{0.5}/\text{N-PC}$ composites showed the strong dark absorption. Finally, after 30 min by switching on the lamp, about 75.44% in 50 min_{total(= 30 min dark+ under solar-simulated light)}, 70.99% in 50 min_{total}, and 72.35% in 45 min_{total} of MO removed on *C Cu*, $\text{Cu}_{0.25}/\text{N-PC}$, and $\text{Cu}_{0.5}/\text{N-PC}$ composites, respectively. Removing MO from *C Cu*, $\text{Cu}_{0.25}/\text{N-PC}$ and $\text{Cu}_{0.5}/\text{N-PC}$ mainly attributed to the photocatalytic activity. For determining photo-degradation rate, the absorption of MO in the dark over the composites was tested (Fig. 7b). The first-order kinetic photocatalytic reaction rate constants of *C Cu*, $\text{Cu}_{0.25}/\text{N-PC}$, and $\text{Cu}_{0.5}/\text{N-PC}$ were calculated as 0.0496, 0.0627, and 0.0551 min⁻¹,

respectively (Table 2). These results indicated that the order of the rate of the photocatalytic activity was $\text{Cu}_{0.25}/N\text{-PC} > \text{Cu}_{0.5}/N\text{-PC} > \text{C Cu}$.

Some controlled experiments were designed to clarify the nature of photocatalytic reaction over the $\text{Cu}_{0.25}/N\text{-PC}$. The rate of the removal of MO was alerted to 0.0020, 0.0006, and 0.0186 min^{-1} in the absence of light ($\text{Cu}_{0.25}/N\text{-PC}$ and H_2O_2), oxidant ($\text{Cu}_{0.25}/N\text{-PC}$ and $h\nu$), and photocatalyst (H_2O_2 and $h\nu$), respectively (Fig. 7a). The rate of the removal of the MO in the absence of light was very low. Accordingly, the $\text{Cu}_{0.25}/N\text{-PC}$ could not catalytic decompose H_2O_2 and produced $\bullet\text{OH}$ radicals. The removal of the MO in the absence of photocatalyst condition (0.0186 min^{-1}) indicates the direct photolysis of H_2O_2 . By adding $\text{Cu}_{0.25}/N\text{-PC}$ composite into the reaction medium, the rate increased around three times (0.0628 min^{-1}) rather than the reaction without the catalyst. This result indicated that H_2O_2 promotes the photocatalysis process by generating $\bullet\text{OH}$ radicals *via* the capturing of the photoinduced electrons in the excited $\text{Cu}_{0.25}/N\text{-PC}$ [36].

The rate of MO removal decreased to 0.0223 min^{-1} when the amount of H_2O_2 was reduced to 0.5 mL (Fig. 7c). An excess amount of H_2O_2 (1.5 mL) retards the rate to 0.0536 min^{-1} . In higher concentration, H_2O_2 acts as the scavenger of $\bullet\text{OH}$ radicals to generated perhydroxy radicals ($\bullet\text{OOH}$) with lower oxidation potential [37].

The photocatalytic activity of the composites on the degradation of Rh B dye was investigated as well (Fig. 8). The C Cu, *N*-PC, $\text{Cu}_{0.125}/N\text{-PC}$, $\text{Cu}_{0.25}/N\text{-PC}$, and $\text{Cu}_{0.5}/N\text{-PC}$ composites absorbed around 2.40%, 91.22%, 75.64%, 1.20%, and 39.00% of Rh B, respectively, in 30 min dark. The *N*-PC and $\text{Cu}_{0.125}/N\text{-PC}$ composites showed the strong dark absorption. After 30 min by switching on the lamp, about 99.04% in $70 \text{ min}_{\text{total}}$,

93.95% in 50 min_{total}, 94.73% in 55 min_{total}, and 95.04% in 60 min_{total} of Rh B removed on C Cu, Cu_{0.125}/*N*-PC, Cu_{0.25}/*N*-PC, and Cu_{0.5}/*N*-PC composites, respectively. The removal of Rh B in C Cu, Cu_{0.25}/*N*-PC and Cu_{0.5}/*N*-PC mainly attributed to the photocatalytic activity. For determining photo-degradation rate, the absorption of Rh B in the dark over composites was investigated (Fig. 8b). The first-order kinetic photocatalytic reaction rate constants of C Cu, Cu_{0.25}/*N*-PC, and Cu_{0.5}/*N*-PC were calculated to 0.1243, 0.1308, and 0.0723 min⁻¹, respectively (Table 3). The rate of the removal of Rh B was alerted in different reaction conditions from 0.0012, 0.0008, and 0.0354 min⁻¹ in the absence of light (Cu_{0.25}/*N*-PC and H₂O₂), oxidant (Cu_{0.25}/*N*-PC and *hν*), and photocatalyst (H₂O₂ and *hν*), respectively (Fig. 8a). The rate decreased to 0.062 and 0.1155 min⁻¹ in 0.5 and 1.5 mL of H₂O₂ (Fig. 8c).

The best photocatalytic activity of Cu_{0.25}/*N*-PC could be attributed to the following reasons: (i) Cu₂O in Cu_{0.25}/*N*-PC was well-crystallized, (ii) BET surface area was higher than Cu_{0.5}/*N*-PC, (iii) the absence of the agglomeration in Cu_{0.25}/*N*-PC toward Cu_{0.5}/*N*-PC (iv) the possible synergetic effects between hollow carbon (from ZIF-8) and Cu₂O (from CuPc) which could be enhanced the intrinsic properties of each component.

The effect of radical scavenger was studied in the degradation of MO dye (Fig. 9a). Hydroxyl radicals play a significant role in the degradation of dye. To investigate the role of hydroxyl radicals, the degradation process was carried out in the presence of hydroxyl radical scavenger like methanol (MeOH) [38]. The photocatalytic activity greatly decreased by adding MeOH (0.01 M_{aq}). The rate constant decreases more than three times from 0.0628 min⁻¹ to 0.0200 min⁻¹. The result showed that the •OH radicals played a significant role in the MO degradation. Iodide ion (I⁻) was reported to be a scavenger of positive holes

(h^+). The photocatalytic effect slightly increased (rate constant = 0.0700 min^{-1}) by adding KI ($0.01 \text{ M}_{\text{aq}}$). Thereby, photo-excited holes acted slightly on dye degradation [39]. Dissolved oxygen can act as a photo-generated electron scavenger to give $\text{O}_2^{\cdot-}$ and $\cdot\text{OH}$ active species [40]; the latter has been proven to be the major oxidation species in this process. To examine the role of $\text{O}_2^{\cdot-}$, benzoquinone (BQ) ($0.01 \text{ M}_{\text{aq}}$) was used as an $\text{O}_2^{\cdot-}$ quencher. Adding BQ could decrease the photocatalytic efficiency of composite (rate constant = 0.0416 min^{-1}), which showed that the MO photo-degradation is caused by $\text{O}_2^{\cdot-}$ to a low degree. The same results were observed in quenching experiments for Rh B. The addition of radical scavenger leads to the change of rate constant from 0.1313 min^{-1} to 0.1418 , 0.0399 , and 0.0653 min^{-1} for KI, MeOH, and BQ (as radical scavengers), respectively (Fig. 9b). In conclusion, the dye degradation on $\text{Cu}_{0.25}/\text{N-PC}$ was attributed to hydroxyl and superoxide radicals.

Based on the above experiments, a possible photocatalytic mechanism for dye degradation was proposed in Fig. 10. In principle, the electrons may transit from valance band (vb) to conduction band (cb) in Cu_2O semiconductor under simulated light irradiation, leading to the generation of e^-/h^+ pairs, which will be separated rapidly and transferred to the surface of Cu_2O (Fig. 10). The electrons reduced O_2 to $\text{O}_2^{\cdot-}$ and H_2O_2 to $\cdot\text{OH}$. The experimental results above illustrate that $\text{Cu}_{0.25}/\text{N-PC}$ composite exhibits the higher photocatalytic activity than C Cu. The hollow carbon structure can strongly enhance the adsorption capacity of $\text{Cu}_{0.25}/\text{N-PC}$ composite. The adsorbed dye molecules are aggregated on the surface of hollow carbon structure. Due to the small size of the dye molecule, it is easy to penetrate the carbon layer [41] and be captured by the reactive species $\text{O}_2^{\cdot-}$ and $\cdot\text{OH}$ radicals, which has a strong oxidizability and can completely degrade dye molecules in the desired efficiency.

The Photoluminescence (PL) emission spectra have been widely used to investigate the efficiency of charge carrier trapping, immigration and transfer, and to understand the fate of e^-/h^+ pairs in semiconductor particles [42]. Furthermore, the better separation of photogenerated e^-/h^+ pairs in the Cu_x/N -PC composite was confirmed by PL emission spectra of C Cu and Cu_x/N -PC composites. In Fig. 11, it was indicated that the Cu_x/N -PC composite exhibited much lower emission intensity than C Cu, indicating that the recombination of the photogenerated charge carrier was inhibited greatly in the Cu/N -PC composite. The efficient charge separation could increase the lifetime of the charge carriers and enhance the efficiency of the interfacial charge transfer to adsorbed substrates, and then account for the higher activity of the Cu/N -PC composite photocatalyst. This result similar to other reports in carbon doped or composites semiconductor metal oxide photocatalyst (such as TiO_2 and ZnO) [41-45].

3.2. The photocatalytic activity of Cu_x/N -PC composites on the C-H activation of formamides

The catalytic activity of Cu_x/N -PC composites was examined in the synthesis of carbamates by C-H activation of formamides. Carbamates have frequently been found in many biologically active products, pharmaceutical drugs, agricultural chemicals as well as foams. They also play a unique role in organic chemistry as valuable intermediates and protecting groups [46]. Traditional methods for the synthesis of these compounds include the reaction of amines with phosgene and its derivatives or the reaction of alcohols with isocyanates. Two main drawbacks of these procedures are toxic and harmful reagents and the generation of by-products. Recently, Kumar *et al.* reported that the $CuBr_2$ catalyzed the

oxidative C-O coupling by C-H activation of formamides to give enol carbamates [47]. The main problem of this reaction is the inability to recycling all catalyst at the end of the reaction. Therefore, we used Cu/*N*-PC composite as a reusable photocatalyst in the synthesis of carbamates by C-H activation of formamides.

We initialized the optimization process using ethyl acetoacetate **1a** (1.0 eq.) and *N,N*-dimethylformamide (DMF) **2a** (27.0 eq.) as coupling partner, and the reaction was performed with Cu_{0.25}/*N*-PC composite (0.02 mol% of Cu) and *tert*-butyl hydroperoxide (TBHP) as oxidant (6 eq.) under the solar-simulated light (Table 4, entry 1). Low yield (15%) was obtained after 4h. The yield increased to 97% by increasing the reaction temperature to 70 °C (Table 4, entry 2). To examine the photocatalyst activity of Cu_{0.25}/*N*-PC, the reaction designed without solar-simulated light and under the thermal condition. The yield decreased to 59% (Table 4, entry 3). Different types of oxidants such as *meta*-chloroperoxybenzoic acid (*m*-CPBA), hydrogen peroxide (H₂O₂), urea hydrogen peroxide (UHP), and cerium ammonium nitrate (CAN) were tested. The results show that none of them have any obvious influence to improve the reaction (Table 4, entries 4-7). Decreasing the amount of the catalyst (0.01 mol% of Cu) leads to the lower yield (Table 4, entry 8). We also used *N*-PC, Cu_{0.125}/*N*-PC, and Cu_{0.5}/*N*-PC composites, in the model reaction. The observed yields of enol carbamate in all cases were surprisingly inferior (Table 4, entries 9-11).

After obtaining the optimum reaction conditions, we evaluated the generality and the scope of substrates for the C-H activation of formamides (Table 5). Various β-ketoesters were used as substrates for the formation of enol carbamates. The nature of the β-ketoesters and formamides did not have any profound influence on the reactivity.

The developed protocol was also applicable to forming different carbamates from 2-carbonyl-substituted phenol (similar to the enol tautomer of β -diketo moiety) (Table 5, entries 16-18). Several formamides reacted smoothly with *ortho*-hydroxyacetophenone in good yields.

Based on the above studies, a plausible mechanism was proved is proposed for the synthesis of enol carbamates using formamide and β -ketoester outlined in Fig. 12. The $\text{Cu}_{0.25}/\text{N-PC}$ composite was subjected to light irradiation, and Cu_2O can be excited and produce photogenerated electron-hole pairs. Then, *t*-BuOOH reduced to *t*-BuO \cdot and OH \cdot by the photogenerated electron in CB. The β -ketoester (**1**) deprotonated by hydroxyl anion and generated copper complex (**i**) with $\text{Cu}_{0.25}/\text{N-PC}$ composite. The *t*-BuO \cdot radical can abstracted hydrogen from the reacting formamide (**2**) and generated the corresponding radical (**ii**). The radical (**ii**) reacted with the copper complex (**i**) and afforded the desired enol carbamate (**3**).

Reusability is an important characteristic of the heterogeneous catalysis which should be examined in the catalytic reaction. Therefore, we performed a reusability test for the $\text{Cu}_{0.25}/\text{N-PC}$ composite in the C-H activation of DMF and ethyl acetoacetate under the optimized conditions. After the reaction completion, the catalyst was collected by centrifuge. By adding a new batch of ethyl acetoacetate and DMF, the recovered composite can be used directly for the next run. This recycling protocol enabled the $\text{Cu}_{0.25}/\text{N-PC}$ to be used for seven runs, furnishing quantitative conversion of substrates without loss of activity and selectivity. Fig. 13a depicted the recovery and reusability of $\text{Cu}_{0.25}/\text{N-PC}$ composite.

Furthermore, no significant change was observed in the morphology of $\text{Cu}_{0.25}/N\text{-PC}$ after the seven runs, which was concluded by the TEM image given in Fig. 13b.

The table 6 provides a comparison of the present method with other reported copper catalytic systems in the C-H bond activation of DMF and ethyl acetoacetate. Clearly, the present catalyst exhibited a simple, high effective, and less time-consuming method for the C-H bond activation.

4. Conclusions

In conclusion, we have successfully demonstrated that the $\text{Cu}_x/N\text{-PC}$ composite is a novel, simple, effective and reusable heterogeneous photocatalyst for the degradation of dyes (MO and Rh B) and the C-H activation of formamides. To study the effect of the weight ratio, the array of carbon composites was prepared. We also used C Cu, *N*-PC, $\text{Cu}_{0.125}/N\text{-PC}$, $\text{Cu}_{0.25}/N\text{-PC}$, and $\text{Cu}_{0.5}/N\text{-PC}$ in the photocatalytic degradation of dyes such as MO and Rh B. While the *N*-PC, $\text{Cu}_{0.125}/N\text{-PC}$, and $\text{Cu}_{0.5}/N\text{-PC}$ composites exhibited high to medium the absorption activity of dyes, the $\text{Cu}_{0.25}/N\text{-PC}$ composite revealed the high photocatalytic activity in the presence of H_2O_2 as the oxidant. The best photocatalytic activity of $\text{Cu}_{0.25}/N\text{-PC}$ could be attributed to the high crystallinity of Cu_2O , high BET surface area, the absence agglomeration, and possible synergetic effects between hollow carbon and Cu_2O . The catalyst showed the high reusability, and can be recycled for several times without considerable loss of activity.

Acknowledgements

We gratefully acknowledge financial support from the Research Council of Shahid Beheshti University and the Iranian National Science Foundation (Proposal No: 94028845).

References

- [1] S. De, A. M. Balu, J. C. van der Waal, R. Luque, Biomass-derived porous carbon materials: synthesis and catalytic applications. *ChemCatChem* 7 (2015) 1608-1629.
- [2] Y. Xia, Z. Yang, R. Mokaya, Templated nanoscale porous carbons. *Nanoscale* 2 (2010) 639-659.
- [3] B. Sakintuna, Y. Yurum, Templated porous carbons: a review article. *Ind. Eng. Chem. Res.* 44 (2005) 2893-2902.
- [4] K. Zhang, Z. Hu, J. Chen, Functional porous carbon-based composite electrode materials for lithium secondary batteries. *J. Energy Chem.* 22 (2013) 214-225.
- [5] J. L. Figueiredo, Functionalization of porous carbons for catalytic applications. *J. Mater. Chem. A* 1 (2013) 9351-9364.
- [6] C. West, C. Elfakir, M. Lafosse, Porous graphitic carbon: A versatile stationary phase for liquid chromatography. *J. Chromatogr. A* 1217 (2010) 3201-3216.
- [7] S. M. Saufi, A. F. Ismail, Fabrication of carbon membranes for gas separation—a review. *Carbon* 42 (2004) 241-259.
- [8] Y. Zheng, J. Liu, J. Liang, M. Jaroniec, S. Z. Qiao, Graphitic carbon nitride materials: controllable synthesis and applications in fuel cells and photocatalysis. *Energy Environ. Sci.* 5 (2012) 6717-6731.

- [9] H. Li, Application of porous carbon macrostructures for water purification. *Prog. Chem.* 28 (2016) 1462-1473.
- [10] Y.-Z. Chen, C. Wang, Z.-Y. Wu, Y. Xiong, Q. Xu, S.-H. Yu, H.-L. Jiang, From bimetallic metal-organic framework to porous carbon: high surface area and multicomponent active dopants for excellent electrocatalysis. *Adv. Mater.* 27 (2015) 5010-5016.
- [11] Y. Zheng, Y. Jiao, M. Jaroniec, Y. Jin, S. Z. Qiao, Nanostructured metal-free electrochemical catalysts for highly efficient oxygen reduction. *Small* 8 (2012) 3550-3566.
- [12] L. Yang, S. Jiang, Y. Zhao, L. Zhu, S. Chen, X. Wang, Q. Wu, J. Ma, Y. Ma, Z. Hu, Boron-doped carbon nanotubes as metal-free electrocatalysts for the oxygen reduction reaction. *Angew. Chem. Int. Ed.* 50 (2011) 7132-7135.
- [13] L. He, F. Weniger, H. Neumann, M. Beller, Synthesis, characterization, and application of metal nanoparticles supported on nitrogen-doped carbon: catalysis beyond electrochemistry. *Angew. Chem. Int. Ed.* 55 (2016) 12582-12594.
- [14] H.-C. Zhou, J. R. Long, O. M. Yaghi, Introduction to metal-organic frameworks. *Chem. Rev.* 112 (2012) 673-674.
- [15] J. L. C. Rowsell, O. M. Yaghi, Metal-organic frameworks: a new class of porous materials. *Micropor. Mesopor. Mat.* 73 (2004) 3-14.
- [16] H. Furukawa, K. E. Cordova, M. O’Keeffe, O. M. Yaghi, The chemistry and applications of metal-organic frameworks. *Science* 341 (2013) 1230444.

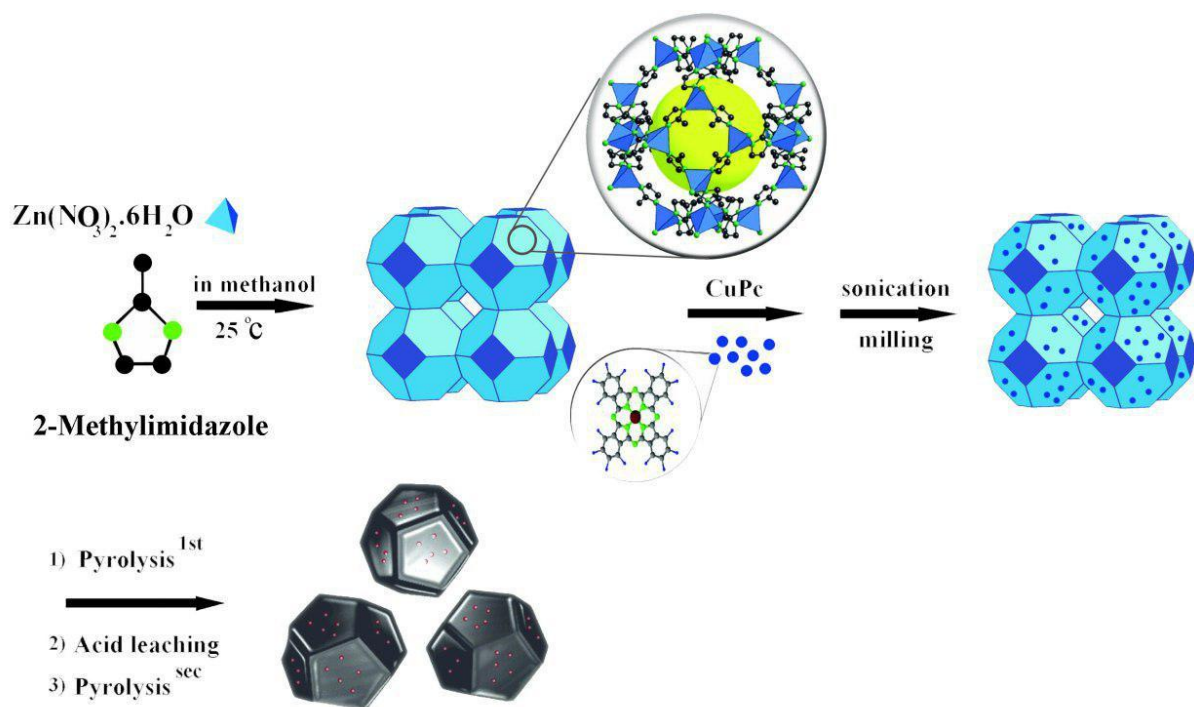
- [17] Y. Deng, Y. Xie, K. Zou, X. Ji, J. Review on recent advances in nitrogen-doped carbons: preparations and applications in supercapacitors. *Mater. Chem. A* 4 (2016) 1144-1173.
- [18] A. Schejn, A. Aboulaich, L. Balan, V. Falk, J. Lalevée, G. Medjahdi, L. Aranda, K. Mozet, R. Schneider, Cu²⁺-doped zeolitic imidazolate frameworks (ZIF-8): efficient and stable catalysts for cycloadditions and condensation reactions. *Catal. Sci. Technol.* 5 (2015) 1829-1839.
- [19] P. Zhang, F. Sun, Z. Xiang, Z. Shen, J. Yun, D. Cao, ZIF-derived in situ nitrogen-doped porous carbons as efficient metal-free electrocatalysts for oxygen reduction reaction. *Energy Environ. Sci.* 7 (2014) 442-450.
- [20] Z. Wang, T. Yan, J. Fang, L. Shi, D. Zhang, Nitrogen-doped porous carbon derived from a bimetallic metal–organic framework as highly efficient electrodes for flow-through deionization capacitors. *J. Mater. Chem. A* 4 (2016) 10858-10868.
- [21] S. Ge, D. Li, S. Huang, W. Chen, G. Tu, S. Yu, Q. He, J. Gong, Y. Li, C. Hong, C. Wu, Z. Zheng, A magnetically recyclable Fe₃O₄@C@TNCuPc composite catalyst for chromogenic identification of phenolic pollutants. *J. Mol. Catal. A: Chem.* 410 (2015) 193-201.
- [22] Z. Zhang, W. Wang, D. Jiang, J. Xu, CuPc sensitized Bi₂MoO₆ with remarkable photo-response and enhanced photocatalytic activity. *Catal. Commun.* 55 (2014) 15-18.
- [23] Z. Zhang, W. Wang, L. Zhang, Large improvement of photo-response of CuPc sensitized Bi₂WO₆ with enhanced photocatalytic activity. *Dalton Trans.* 42 (2013) 4579-4585.

- [24] Z. Wang, H. Chen, P. Tang, W. Mao, F. Zhang, G. Qian, X. Fan, Hydrothermal in situ preparation of the copper phthalocyanine tetrasulfonate modified titanium dioxide photocatalyst. *Colloids Surf. A* 289 (2006) 207-211.
- [25] Z. Han, X. Han, X. Zhao, J. Yu, H. Xu, Iron phthalocyanine supported on amidoximated PAN fiber as effective catalyst for controllable hydrogen peroxide activation in oxidizing organic dyes. *J. Hazard. Mater.* 2016, 320, 27-35.
- [26] G. Schulz, R. Polster, Production of copper phthalocyanines. US3412102 (A), 1968.
- [27] R. Zheng, S. Liao, S. Hou, X. Qiao, G. Wang, L. Liu, T. Shu, L. Du, A hollow spherical doped carbon catalyst derived from zeolitic imidazolate framework nanocrystals impregnated/covered with iron phthalocyanines. *J. Mater. Chem. A* 4 (2016) 7859-7868.
- [28] M. Wang, X. Xu, Y. Liu, Y. Li, T. Lu, L. Pan, From metal-organic frameworks to porous carbons: A promising strategy to prepare high-performance electrode materials for capacitive deionization. *Carbon* 108 (2016) 433-439.
- [29] B. Chen, R. Li, G. Ma, X. Gou, Y. Zhu, Y. Xia, Cobalt sulfide/*N,S* codoped porous carbon core-shell nanocomposites as superior bifunctional electrocatalysts for oxygen reduction and evolution reactions. *Nanoscale* 7 (2015) 20674-20684.
- [30] S. K. Movahed, M. Dabiri, A. Bazgir, A one-step method for preparation of Cu@Cu₂O nanoparticles on reduced graphene oxide and their catalytic activities in *N*-arylation of *N*-heterocycles. *Appl. Catal. A: General* 481 (2014) 79-88.
- [31] T. Toyao, M. Fujiwaki, K. Miyahara, T.-H. Kim, Y. Horiuchi, M. Matsuoka, Design of zeolitic imidazolate framework derived nitrogen-doped nanoporous carbons

- containing metal species for carbon dioxide fixation reactions. *ChemSusChem* 8 (2015) 3905-3912.
- [32] Q. He, X. Yang, R. He, A. Bueno-López, H. Miller, X. Ren, W. Yang, B. E. Koel, Electrochemical and spectroscopic study of novel Cu and Fe-based catalysts for oxygen reduction in alkaline media. *J. Power Sources* 213 (2012) 169-179.
- [33] L. Ding, J. Qiao, X. Dai, J. Zhang, J. Zhang, B. Tian, Highly active electrocatalysts for oxygen reduction from carbon-supported copper-phthalocyanine synthesized by high temperature treatment. *Int. J. Hydrogen Energy* 37 (2012) 14103-14113.
- [34] G. Leofanti, M. Padovan, G. Tozzola, B. Venturelli, Surface area and pore texture of catalysts. *Catal. Today* 41 (1998) 207-219.
- [35] A. Aijaz, N. Fujiwara, Q. Xu, From Metal-organic framework to nitrogen-decorated nanoporous carbons: high CO₂ uptake and efficient catalytic oxygen reduction. *J. Am. Chem. Soc.* 136 (2014) 6790-6793.
- [36] Q. Xia, X. Yu, H. Zhao, S. Wang, H. Wang, Z. Guo, H. Xing, Syntheses of novel lanthanide metal-organic frameworks for highly efficient visible-light-driven dye degradation. *Cryst. Growth Des.* 17 (2107) 4189-4195
- [37] L. Ai, C. Zhang, L. Li, J. Jiang, Iron terephthalate metal-organic framework: revealing the effective activation of hydrogen peroxide for the degradation of organic dye under visible light irradiation. *Appl. Catal. B* 148-149 (2014) 191-200.
- [38] L. G. Devi, S. G. Kumar, K. M. Reddy, C. Munikrishnappa, Photo degradation of methyl orange an azo dye by advanced fenton process using zero valent metallic

- iron: influence of various reaction parameters and its degradation mechanism. *J. Hazard. Mater.* 164 (2009) 459-467.
- [39] P. Liang, C. Zhang, H. Sun, S. Liu, M. Tadó, S. Wang, Photocatalysis of C, N-doped ZnO derived from ZIF-8 for dye degradation and water oxidation. *RSC Adv.* 6 (2016) 95903-95909.
- [40] Y. Li, J. Wang, H. Yao, L. Dang, Z. Li, Efficient decomposition of organic compounds and reaction mechanism with BiOI photocatalyst under visible light irradiation. *J. Mol. Catal. A: Chem.* 334 (2011) 116-122.
- [41] T. Chen, S. Yu, X. Fang, H. Huang, L. Li, X. Wang, H. Wang, Enhanced photocatalytic activity of C@ZnO core-shell nanostructures and its photoluminescence property. *Appl. Surf. Sci.* 389 (2106) 303-310.
- [42] Y. Yu, J. C. Yu, J.-G. Yu, Y.-C. Kwok, Y.-K. Che, J.-C. Zhao, L. Ding., W.-K. Ge, P.-K. Wong, Enhancement of photocatalytic activity of mesoporous TiO₂ by using carbon nanotubes. *Appl. Catal. A: General* 289 (2005) 186–196.
- [43] J. Mu, C. Shao, Z. Guo, Z. Zhang, M. Zhang, P. Zhang, B. Chen, Y. Liu, High photocatalytic activity of ZnO-Carbon nanofiber heteroarchitectures. *ACS Appl. Mater. Interfaces* 3 (2011) 590–596
- [44] J. Yu, T. Ma, S. Liu, Enhanced photocatalytic activity of mesoporous TiO₂ aggregates by embedding carbon nanotubes as electron-transfer channel. *Phys. Chem. Chem. Phys.*, 13 (2011) 3491–3501
- [45] W. Ren, Z. Ai, F. Jia, L. Zhang, X. Fan, Z. Zou, Low temperature preparation and visible light photocatalytic activity of mesoporous carbon-doped crystalline TiO₂. *Appl. Catal. B: Environmental* 69 (2007) 138–144.

- [46] D. Saberi, A. Heydari, CuO nanoparticles supported on α -Fe₂O₃-modified CNTs: a magnetically separable catalyst for oxidative C–O coupling of formamides with 1,3-dicarbonyl compounds. *Tetrahedron Lett.* 54 (2013) 4178-4180.
- [47] G. S. Kumar, C. U. Maheswari, R. A. Kumar, M. L. Kantam, K. R. Reddy, Copper-catalyzed oxidative C-O coupling by direct C-H bond activation of formamides: synthesis of enol carbamates and 2-carbonyl-substituted phenol carbamates. *Angew. Chem. Int. Ed.* 50 (2011) 11748-11751.
- [48] D. Saberi, S. Mansoori, E. Ghaderi, K. Niknam, Copper nanoparticles on charcoal: an effective nanocatalyst for the synthesis of enol carbamates and amides via an oxidative coupling route. *Tetrahedron Lett.* 57 (2016) 95–99
- [49] B. D. Barve, Y. C. Wu, M. El- Shazly, D. W. Chuang, Y. M. Chung, Y. H. Tsai, S. F. Wu, M. Korinek, Y. C. Du, C. T. Hsieh, J. J. Wang, Synthesis of carbamates by direct c–h bond activation of formamides. *Eur. J. Org. Chem.* (2012) 6760–6766.



Scheme 1. Schematic diagram illustrating the synthesis of Cu/N-PC composite

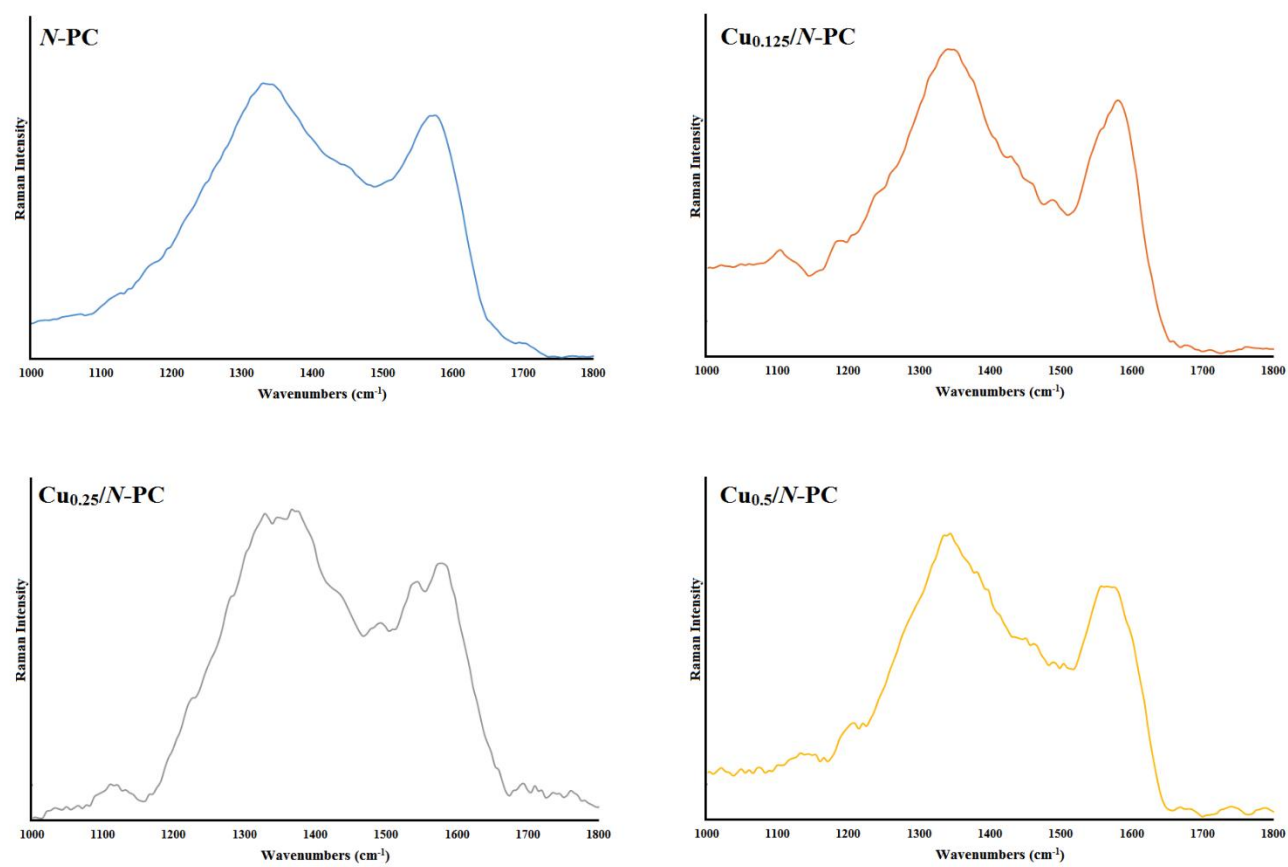


Fig. 1 Raman spectra of *N-PC*, *Cu_{0.125}/N-PC*, *Cu_{0.25}/N-PC* and *Cu_{0.5}/N-PC* composites

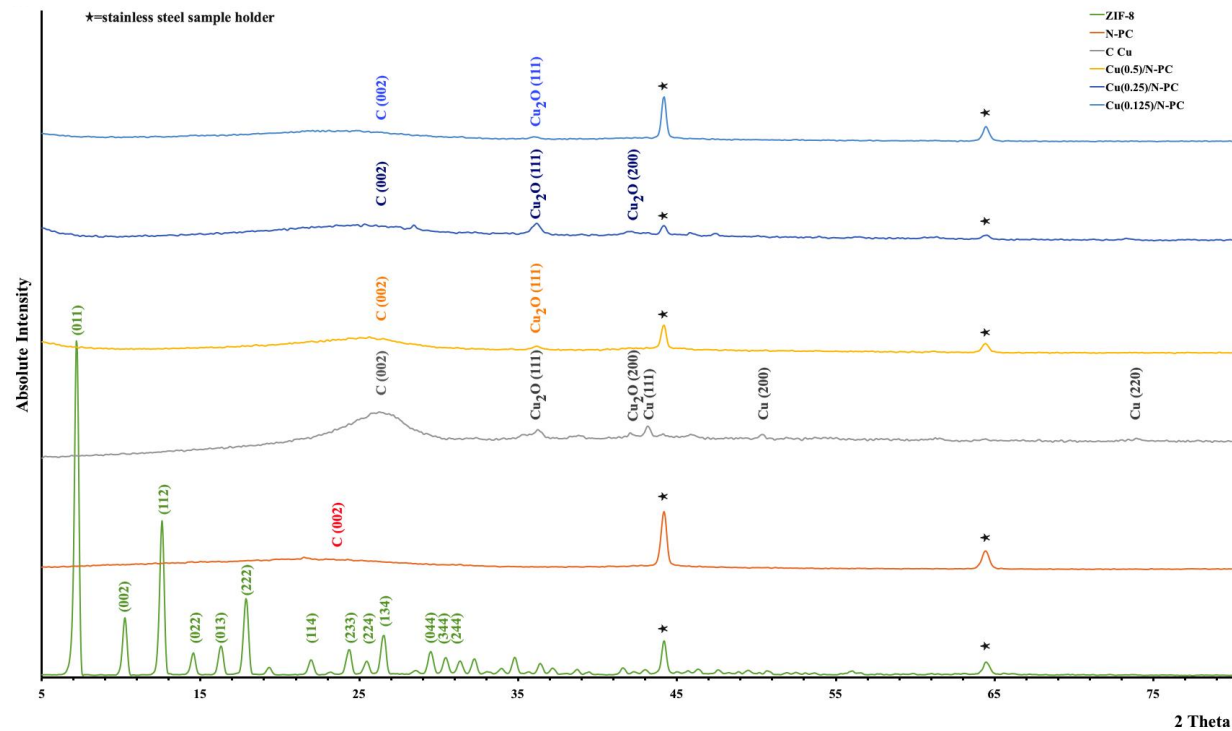


Fig. 2 XRD patterns of ZIF-8, N-PC, C Cu, Cu_{0.125}/N-PC, Cu_{0.25}/N-PC and Cu_{0.5}/N-PC composites.

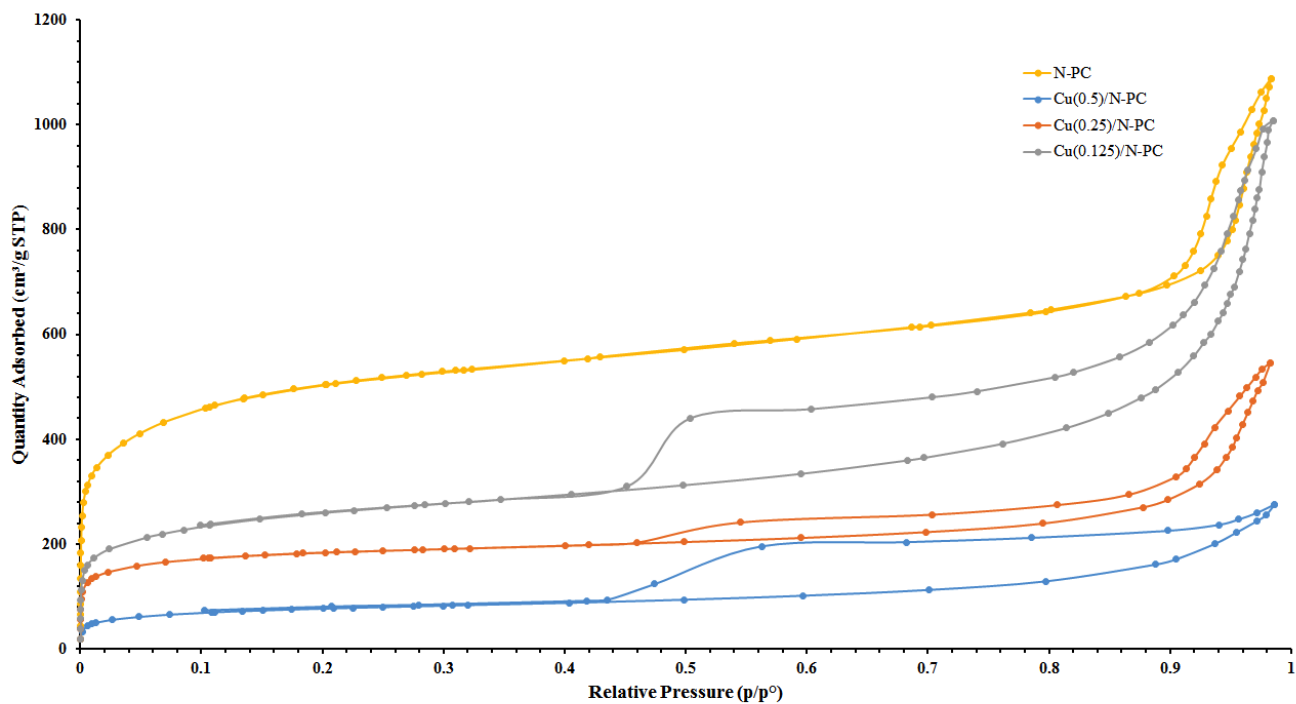


Fig. 3 Nitrogen adsorption–desorption isotherms of *N*-PC, Cu_{0.125}/*N*-PC, Cu_{0.25}/*N*-PC and Cu_{0.5}/*N*-PC composites.

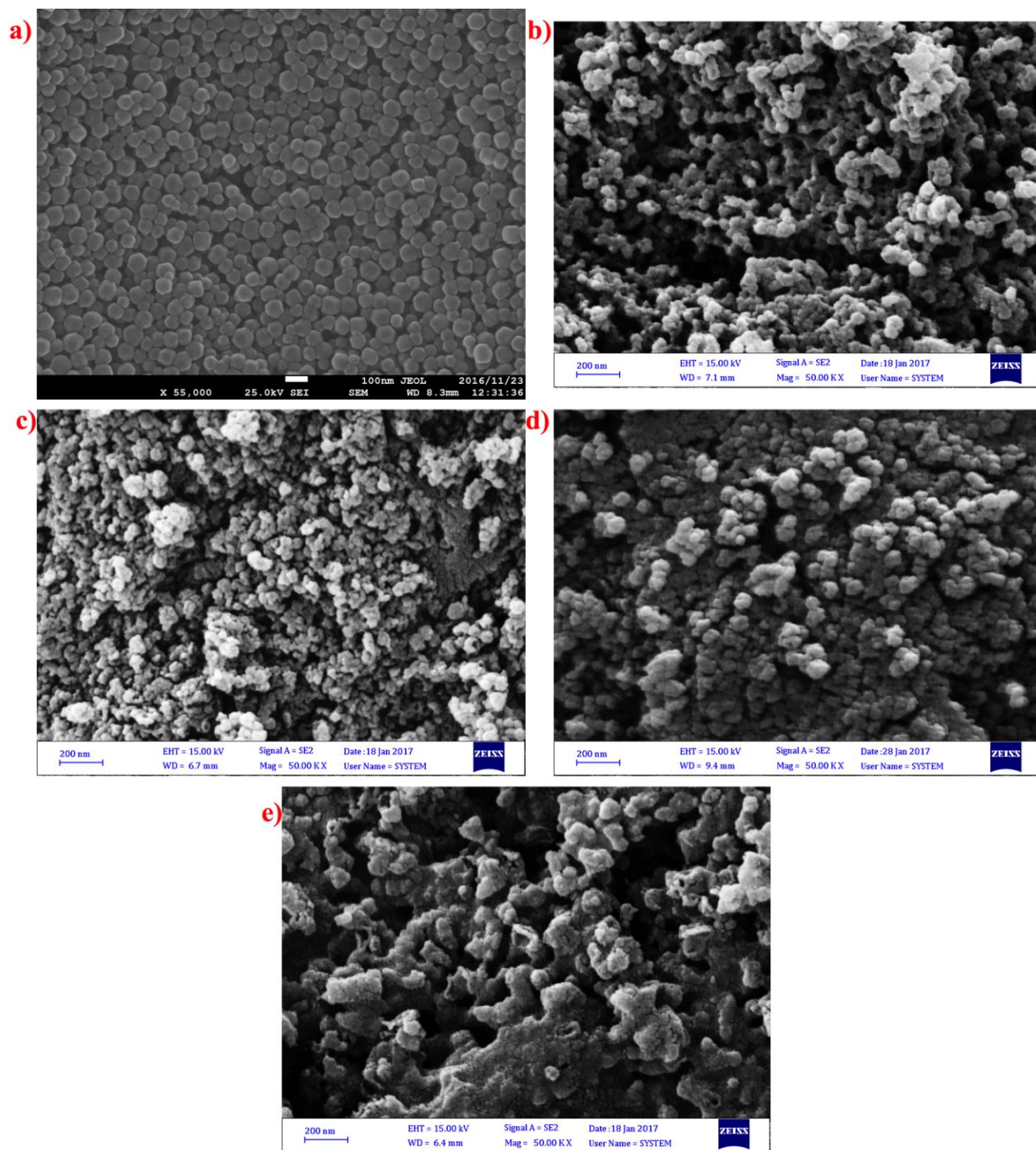


Fig. 4 FESEM images of a) ZIF-8 (scale bar = 100 nm), b) *N*-PC(scale bar = 200 nm), c) $\text{Cu}_{0.125}/N\text{-PC}$ (scale bar = 200 nm), d) $\text{Cu}_{0.25}/N\text{-PC}$ (scale bar = 200 nm), and e) $\text{Cu}_{0.5}/N\text{-PC}$ (scale bar = 200 nm) composites.

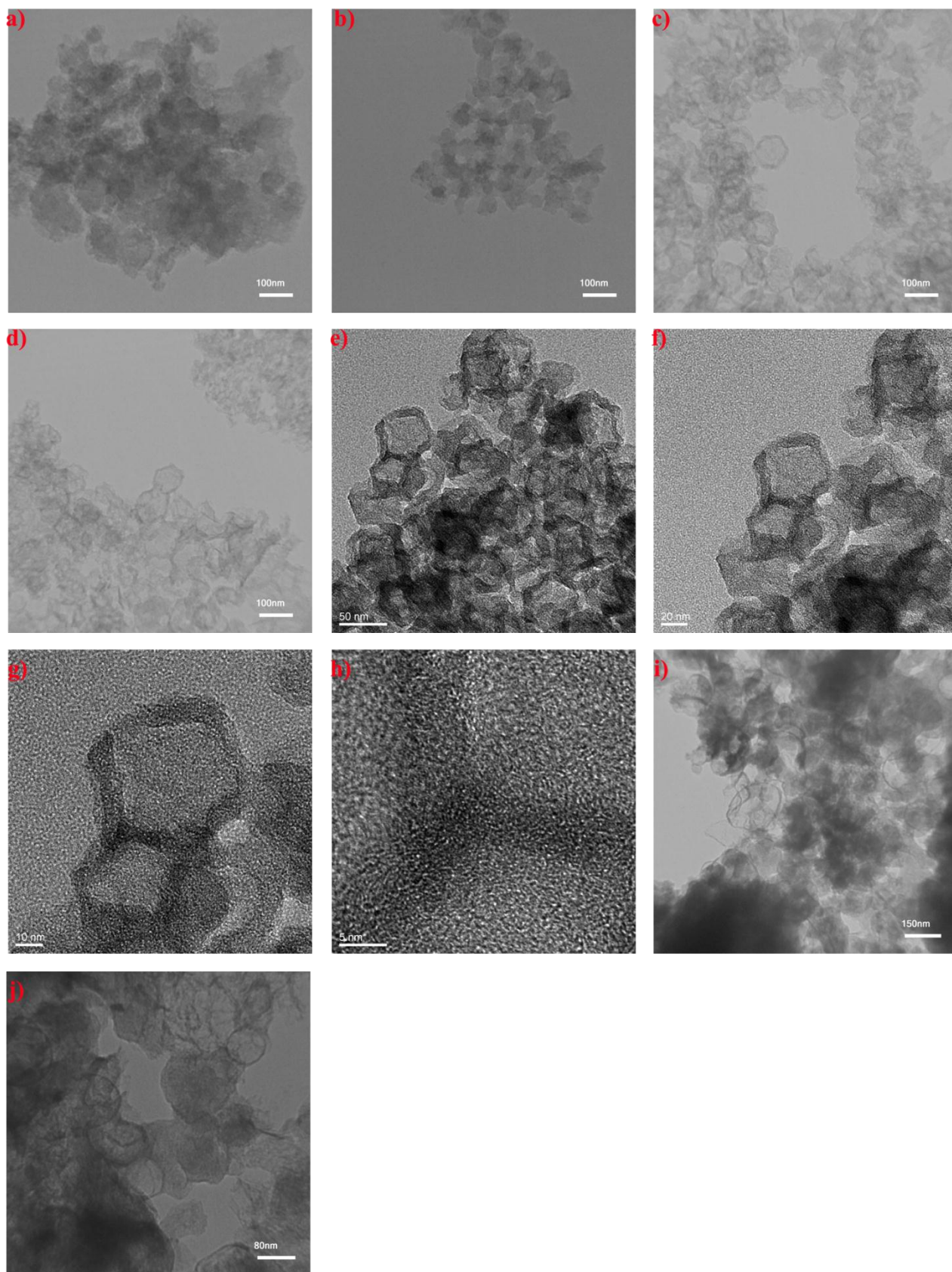
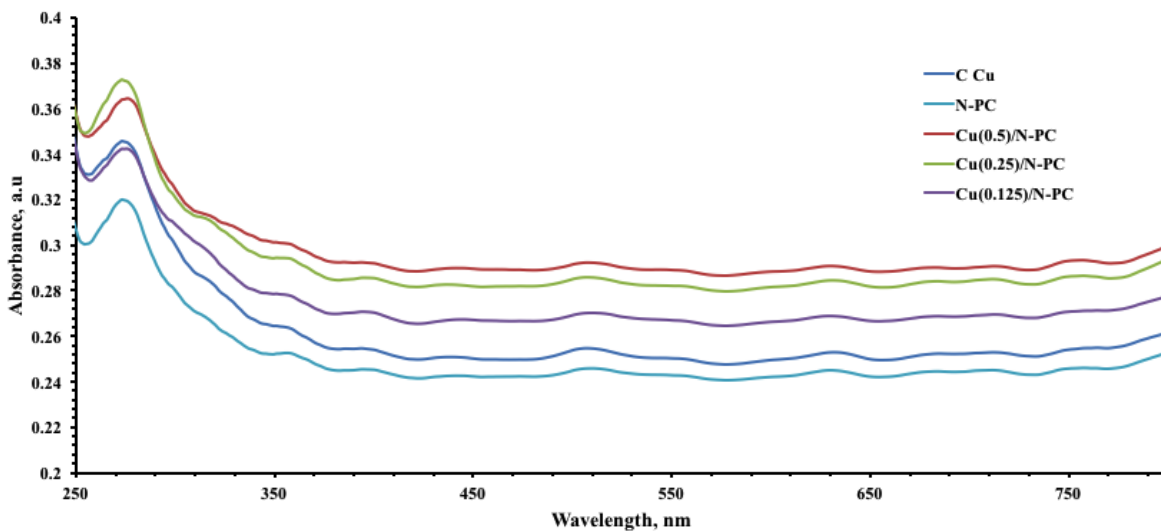


Fig. 5 TEM and HR-TEM images of a-b) *N*-PC (scale bar = 100 nm), c-d) Cu_{0.125}/*N*-PC (scale bar = 100 nm), e-h) Cu_{0.25}/*N*-PC (scale bar e= 50 nm, f= 20 nm, g = 10 nm, and h = 5 nm,) and i-j) Cu_{0.5}/*N*-PC composites (scale bar i= 150 nm and j= 80 nm)

a)



b)

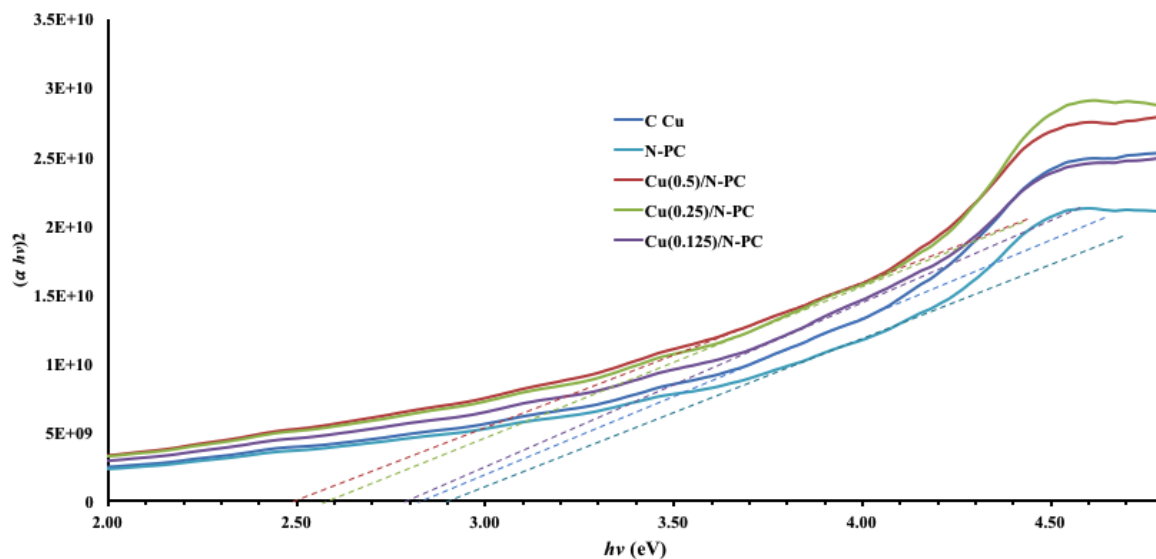


Fig. 6 a) DRS spectra of *N*-PC, C Cu, Cu_{0.125}/*N*-PC, Cu_{0.25}/*N*-PC and Cu_{0.5}/*N*-PC composites, b) Plots of $(\alpha h\nu)^2$ vs photon energy of *N*-PC, C Cu, Cu_{0.125}/*N*-PC, Cu_{0.25}/*N*-PC and Cu_{0.5}/*N*-PC composites.

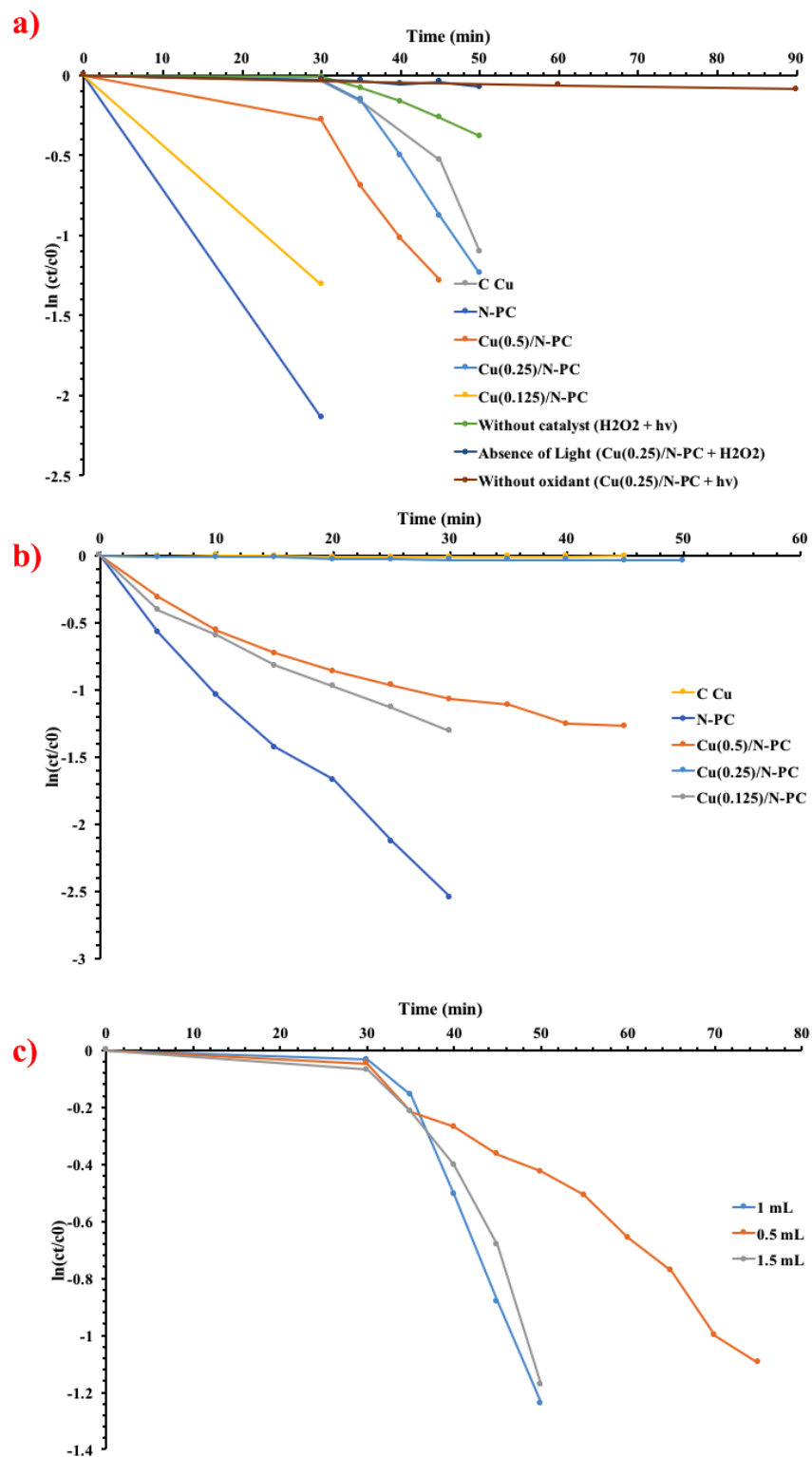


Fig. 7 Plot of $\ln(C_t/C_0)$ against the reaction time a) the removal of MO over of *N*-PC, C Cu, Cu_{0.125}/*N*-PC, Cu_{0.25}/*N*-PC and Cu_{0.5}/*N*-PC composites and control experiments: absence

light ($\text{Cu}_{0.25}/N\text{-PC}$ and H_2O_2), without oxidant ($\text{Cu}_{0.25}/N\text{-PC}$ and $h\nu$), and without photocatalyst (H_2O_2 and $h\nu$), b) the absorption of MO over of $N\text{-PC}$, C Cu , $\text{Cu}_{0.125}/N\text{-PC}$, $\text{Cu}_{0.25}/N\text{-PC}$ and $\text{Cu}_{0.5}/N\text{-PC}$ composites, and c) the effect of the concentration of H_2O_2 over of $\text{Cu}_{0.25}/N\text{-PC}$ composite.

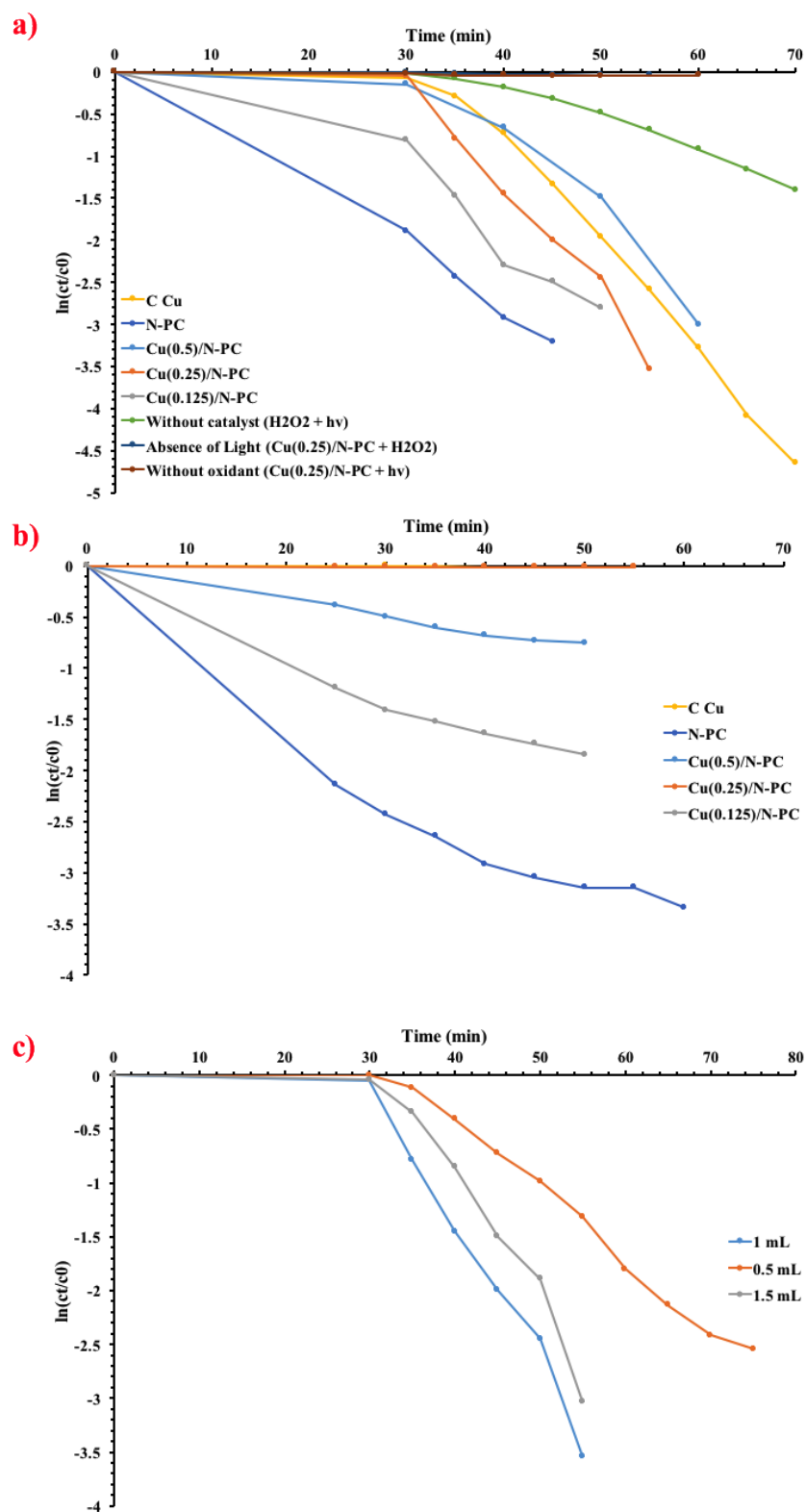


Fig. 8 Plot of $\ln(C_t/C_0)$ against the reaction time a) the removal of Rh B over of *N*-PC, C Cu, $Cu_{0.125}/N$ -PC, $Cu_{0.25}/N$ -PC and $Cu_{0.5}/N$ -PC composites and control experiments:

absence light ($\text{Cu}_{0.25}/N\text{-PC}$ and H_2O_2), without oxidant ($\text{Cu}_{0.25}/N\text{-PC}$ and $h\nu$), and without photocatalyst (H_2O_2 and $h\nu$), b) the absorption of RhB over of $N\text{-PC}$, Cu , $\text{Cu}_{0.125}/N\text{-PC}$, $\text{Cu}_{0.25}/N\text{-PC}$ and $\text{Cu}_{0.5}/N\text{-PC}$ composites, and c) the effect of the concentration of H_2O_2 over of $\text{Cu}_{0.25}/N\text{-PC}$ composite.

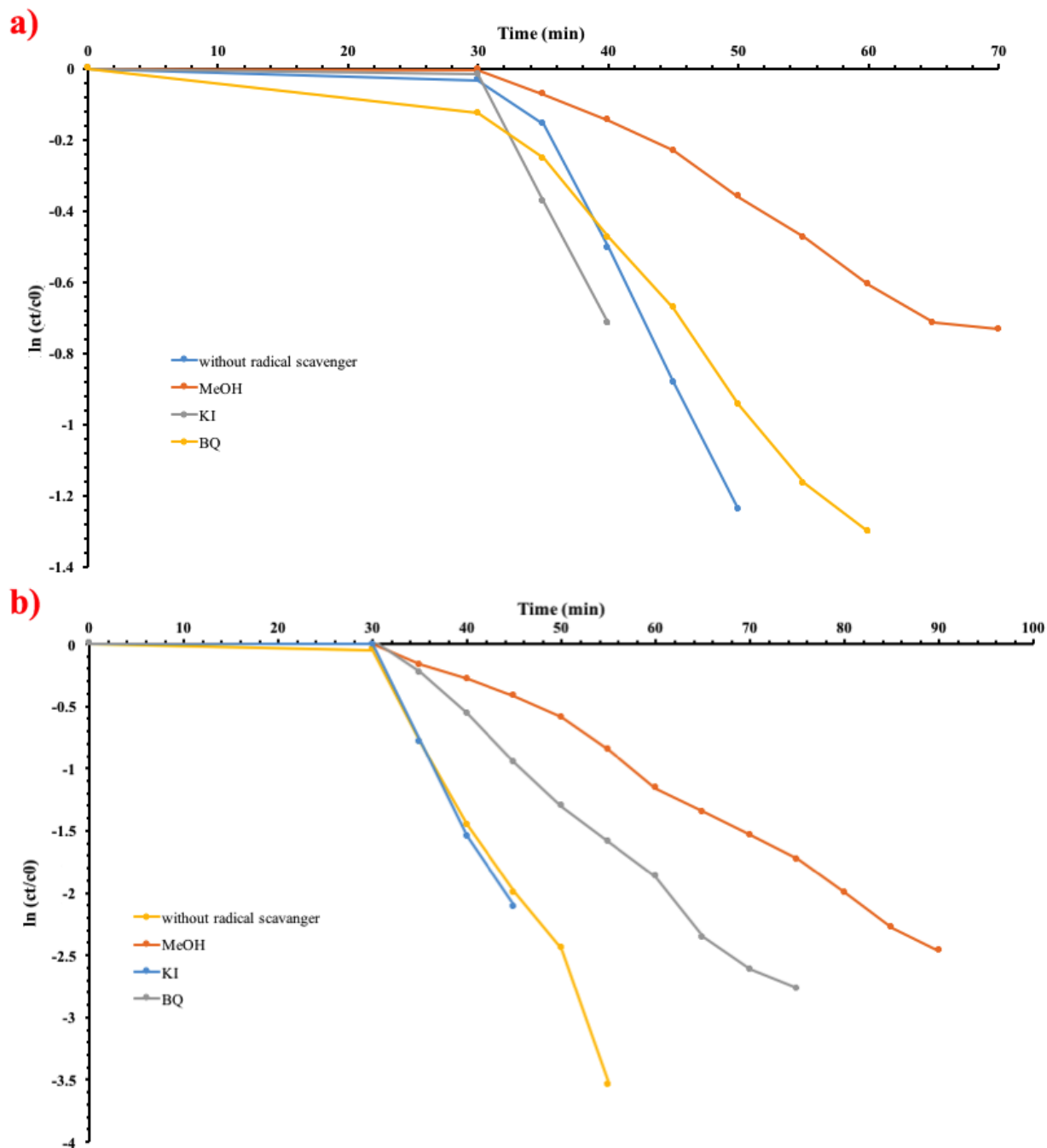


Fig. 9 The quenching tests with the addition of MeOH, KI, and BQ for a) MO and b) Rh
B.

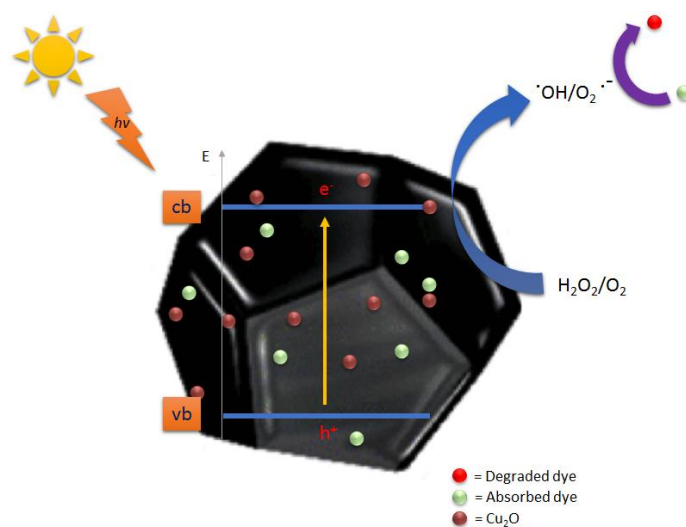


Fig. 10 Schematic mechanism for the degradation of dyes on Cu_{0.25}/N-PC composite in the presence of H₂O₂ under simulated light irradiation.

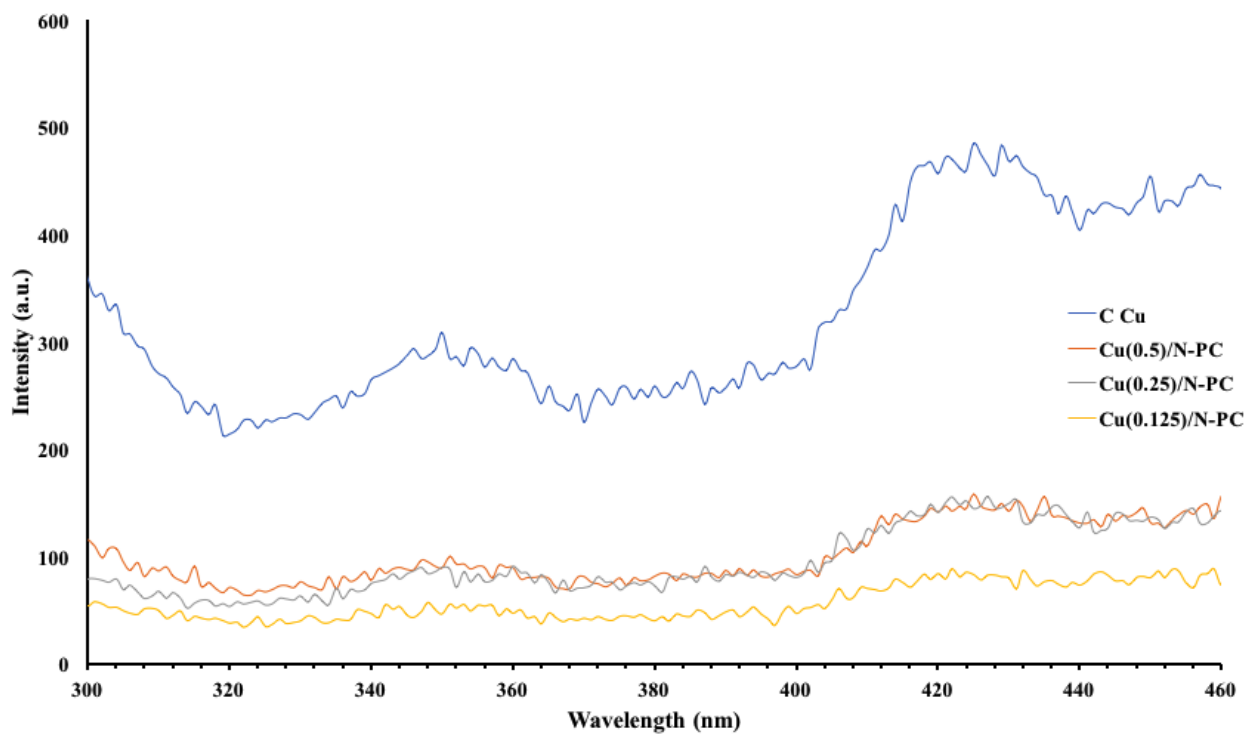


Fig. 11 PL emission spectra of C Cu, Cu_{0.5}/N-PC, Cu_{0.25}/N-PC, and Cu_{0.125}/N-PC composites

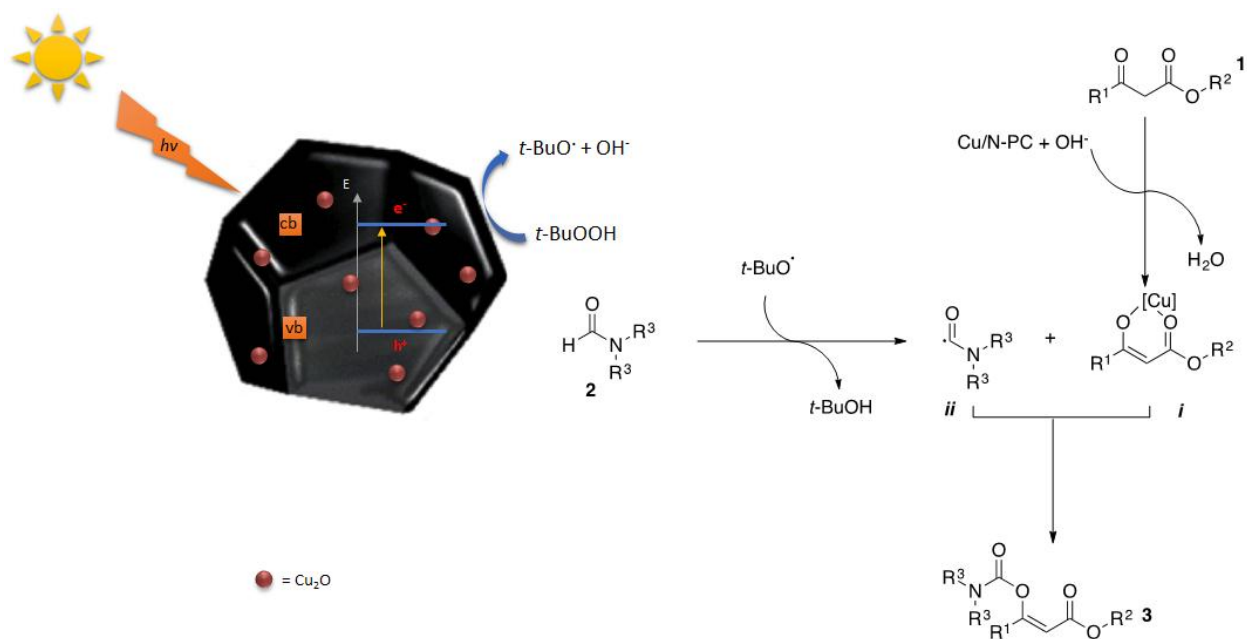


Fig. 12 Mechanism for the coupling of formamide with β -ketoester in the presence of Cu_{0.25}/N-PC composite under simulated light irradiation.

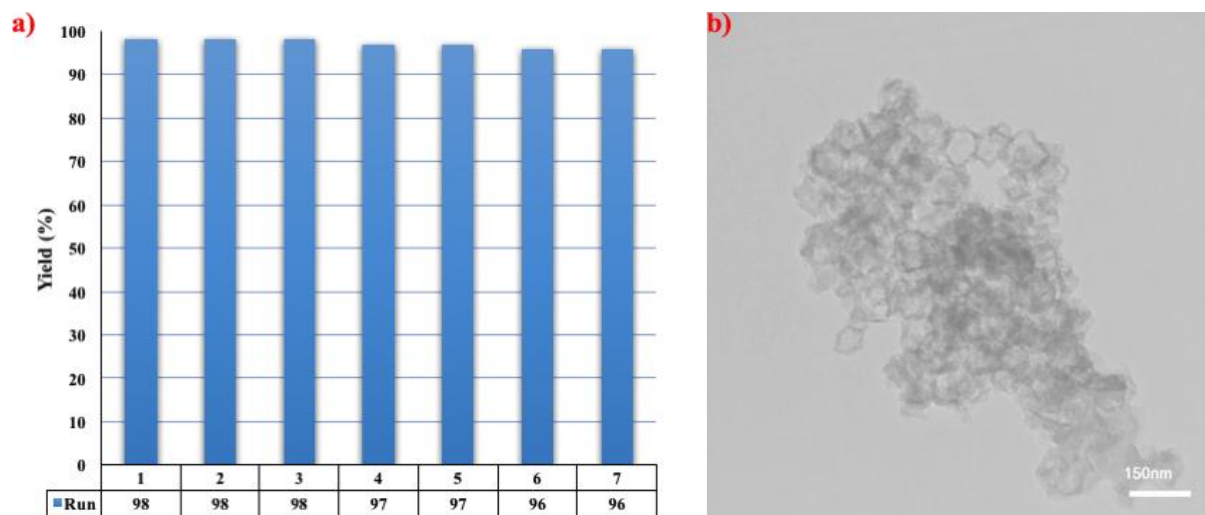


Fig. 13 a) Recycling of the $\text{Cu}_{0.25}/\text{N-PC}$ composite in the C-H activation of DMF and ethyl acetoacetate; b) TEM image of the composite after 7 runs (scale bar = 150 nm).

Table 1. Surface area analysis parameters of N-PC , $\text{Cu}_{0.125}/\text{N-PC}$, $\text{Cu}_{0.25}/\text{N-PC}$ and $\text{Cu}_{0.5}/\text{N-PC}$ composites.

	BET Surface Area (m^2/g)	Langmuir Surface Area (m^2/g)	Pore Volume (cm^3/g)	Micropore Volume (cm^3/g)
N-PC	1613.6090	3854.9964	1.229203	0.393464
$\text{Cu}_{0.125}/\text{N-PC}$	868.8935	3449.8342	1.048987	0.160608
$\text{Cu}_{0.25}/\text{N-PC}$	585.7566	1783.4158	0.586141	0.186520
$\text{Cu}_{0.5}/\text{N-PC}$	256.0843	990.2597	0.334947	0.048145

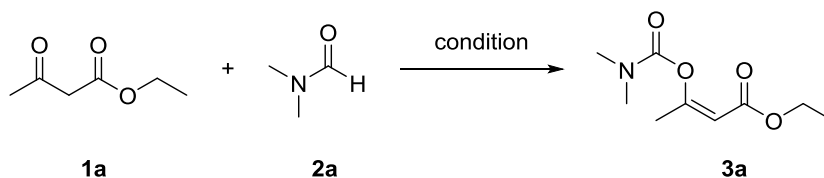
Table 2. The rate constant for absorption (dark), photo-degradation, and total (absorption+photo-degradation) for the removal of the MO dye.

	C Cu	N-PC	Cu _{0.125} /N-PC	Cu _{0.25} /N-PC	Cu _{0.5} /N-PC
Absorption rate (min⁻¹)	0.0003	0.0711	0.0436	0.0001	0.0148
Photo-degradation rate (min⁻¹)	0.0496	-	-	0.0627	0.0551
Total (min⁻¹)	0.0499	0.0711	0.0436	0.0628	0.0699

Table 3. The rate constant for absorption (dark), photo-degradation, and total (absorption+photo-degradation) for the removal of the Rh B dye.

	C Cu	N-PC	Cu _{0.125} /N-PC	Cu _{0.25} /N-PC	Cu _{0.5} /N-PC
Absorption rate (min⁻¹)	0.0040	0.0365	0.0217	0.0005	0.0217
Photo-degradation rate (min⁻¹)	0.1243	0.0317	0.0783	0.1308	0.0723
Total (min⁻¹)	0.1283	0.0682	0.1000	0.1313	0.0940

Table 4. Optimization of reaction conditions for the C-H activation of DMF^a



Entry	Oxidant	Catalyst (mol% of Cu)	Temp. (°C)	Yield (%) ^b
-------	---------	-----------------------	------------	------------------------

1 ^c	TBHP	0.02	r. t.	15
2	TBHP	0.02	70	98
3 ^d	TBHP	0.02	70	59
4	<i>m</i> -CPBA	0.02	70	16
5	H ₂ O ₂	0.02	70	n. r.
6	UHP	0.02	70	n. r.
7	CAN	0.02	70	n. r.
8	TBHP	0.01	70	47
9 ^e	TBHP	-	70	0
10 ^f	TBHP	0.02	70	10
11 ^g	TBHP	0.02	70	53

^a ethyl acetoacetate **1a** (1 mmol), DMF **2a** (27 mmol), oxidant (6 mmol), 30 min, Cu_{0.25}/*N*-PC (x mol% of Cu), under the solar-simulated light.

^b Isolated yield.

^c 4h.

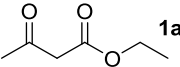
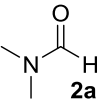
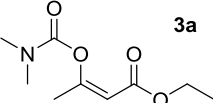
^d under the thermal condition.

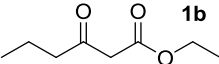
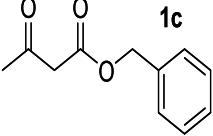
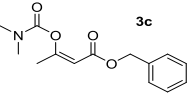
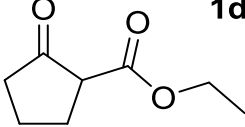
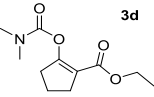
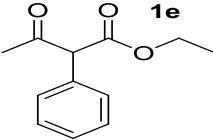
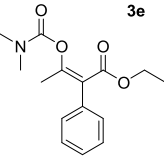
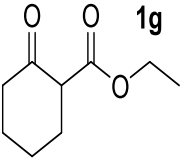
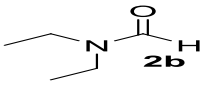
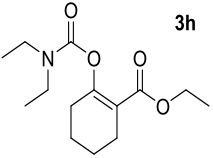
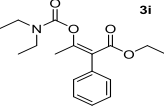
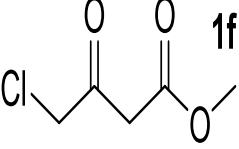
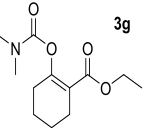
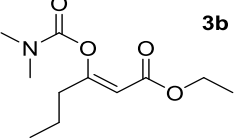
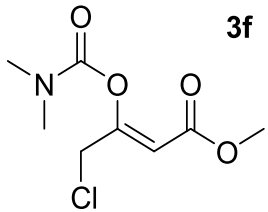
^e *N*-PC.

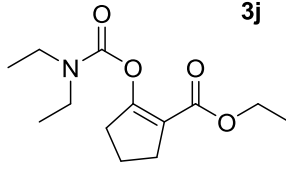
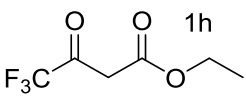
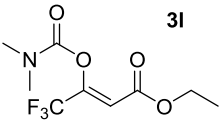
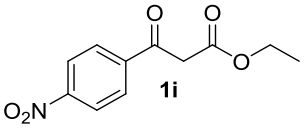
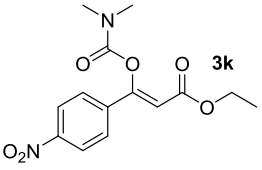
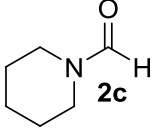
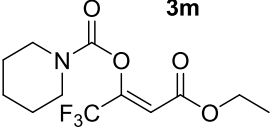
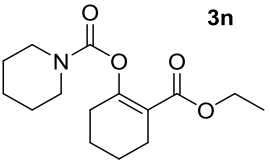
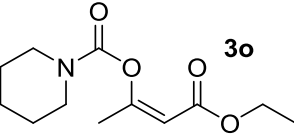
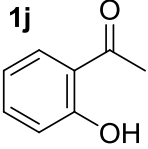
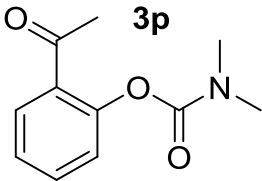
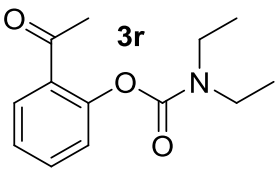
^f Cu_{0.125}/*N*-PC.

^g Cu_{0.5}/*N*-PC.

Table 5. Cu_{0.25}/*N*-PC composite catalyzed C-H activation of formamides^a

Entry	β -ketoesters or <i>ortho</i> -hydroxyacetophenone	Formamide	Product	Yield (%) ^b
1				98

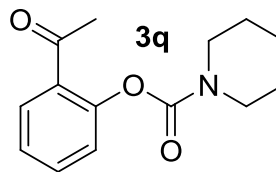
2		1b	2a		1c	92
3		3c	2a		1d	95
4		3d	2a		1e	83
5		3e	2a		1g	90
6		2b	2a		3h	92
7		3i	2a		1f	89
8	1g		3g		3b	85
9	1e	2b		3f	83	

10	1d	2b		3j	76
11		2a		3i	74
12		2a		3k	85
13	1h			3m	61
14	1g	2c		3n	88
15	1a	2c		3o	84
16		2a		3p	98
17	1j	2b		3r	95

18

1j

2c



89

^a β -ketoester (2 mmol), formamide (54 mmol), TBHP (12 mmol), 30 min, 70 °C, under the solar-simulated light, Cu_{0.25}/*N*-PC (0.02 mol% of Cu)

^b Isolated yield.

Table 6. Comparison of efficiency of various copper catalysts in for the C-H bond activation of DMF and ethyl acetoacetate

Catalyst	Condition	Yield (%)	Time (h)	Ref.
Cu _{0.25} / <i>N</i> -PC (0.02 mol%)	TBHP (6 eq.), 70 °C, under the solar- simulated light	98	0.5	This work
Cu/C (1.84 mol%)	TBHP (1.5 eq.), 80 °C	82	5	48
CuBr ₂ (5 mol%)	TBHP (1.5 eq.), 80 °C	73	3	47
CuCl (1 mol%)	TBHP (6 eq.), 70 °C	99	0.5	49